Engineering Fracture Mechanics 224 (2020) 106818

Contents lists available at ScienceDirect

Engineering Fracture Mechanics

journal homepage: www.elsevier.com/locate/engfracmech

Fracture of 3D-printed polymers: Crucial role of filament-scale geometric features

James Allum, Andrew Gleadall*, Vadim V. Silberschmidt

Wolfson School of Mechanical, Electrical and Manufacturing Engineering, Loughborough University, Loughborough LE11 3TU, UK

ARTICLE INFO

Keywords:
Additive Manufacturing
Fused Deposition Modelling
Interface
Bond Strength
Mechanical Properties

ABSTRACT

Is mechanical anisotropy in extrusion-based 3D-printed parts caused by weak inter-filament bonding, as is widely accepted? This study demonstrates that filament-scale geometric features may be a more important factor than filament bonding. Specially designed 3D-printed compact tension specimens were tested normal to, and along, the direction of extruded filaments. Higher strength and toughness were found in the filament direction. These differences disappeared when small grooves, comparable to micro-features, were introduced in specimens tested along the former direction to replicate grooves that naturally occur between filaments/layers. Mechanical testing and fractography demonstrate that filament-scale geometric stress raisers are critically important and cause anisotropy in 3D-printed materials.

1. Introduction

Extrusion-based 3D-printing has emerged as a highly valuable tool for design and manufacturing industries in recent years. 3D-printing enables the manufacture of components with highly intricate geometries that would be extremely complex or impossible to achieve with traditional manufacturing methods such as milling or injection moulding. Extrusion-based 3D-printing of polymers is the most affordable form of additive manufacturing and is utilised in a number of biomedical applications, including three-dimensional virtual surgical planning, generation of anatomical models and manufacturing of patient-specific implants (PSIs) [1,2]. Examples of PSIs include orthopaedic plates for reconstructive surgery and prosthetic bone implants. The biopolymer polylactide (PLA) is one of the most commonly utilised 3D-printing materials. It is a bioabsorbable material, currently employed for bone-repair fixation devices in the healthcare industry [3,4]. Structural integrity of such parts is crucial for success of medical procedures and the healing process, and is highly dependent on the filament-scale geometry [5].

In extrusion-based 3D-printing, a filament is fed into a heated extrusion nozzle, which melts and deposits it onto a build plate. Layers are extruded on top of one another, and each layer is formed of individual extruded filaments; this process repeats until the geometry is complete. As a result of the layer-by-layer approach, a part manufactured by extrusion-based 3D-printing exhibits anisotropic mechanical behaviour, with higher strength in the layer plane and reduced strength between multiple layers; this is a key mechanical limitation of 3D-printed parts, as demonstrated in a number of studies [6–14]. A study by Ahn in 2002 [6] highlighted that anisotropy is direction (and therefore toolpath) dependent.

A vital element of 3D-printing is the dedicated software utilised to convert a CAD model of the part into a toolpath. The software generates machine control code, which is interpreted by the 3D-printer to manufacture the physical structure. Prior to fabrication, the software enables the operator to modify parameters to adjust the manufacturing strategy. These include nozzle temperature, travel

* Corresponding author.
E-mail address: a.gleadall@lboro.ac.uk (A. Gleadall).

https://doi.org/10.1016/j.engfracmech.2019.106818
Received 21 December 2018; Received in revised form 7 August 2019; Accepted 14 December 2019
Available online 20 December 2019
0013-7944/

speed of the printhead, infill raster pattern, extruded filament width and layer height. Numerous studies have been undertaken to provide better understanding of the effect of parameter modifications on the resulting mechanical properties of generated parts and to improve interfacial bond strength [6–27]. It has been widely demonstrated that mechanical properties can be improved by increasing nozzle temperature [15–19]. However, there are conflicting findings with regards to the impact of layer height and travel speed of the printhead. A number of studies showed an increase in strength with decreasing layer height [15–18,20–22], but this was disputed by other studies [6,23,24]. Some works found that decreasing the travel speed of the printhead resulted in increased strength [25–27], but an opposite trend was established in others [24,28]. There have also been a small number of studies that analysed the effects of changing extruded-filament width on resulting strength of 3D-printed components [15,20]. Contradictions within the literature demonstrate the need for more fundamental understanding of factors governing mechanical properties.

It is likely that many of the conflicts between studies are due to the complexity of the 3D-printing process. Most studies investigating the mechanical properties of extrusion-based 3D-printed parts do not isolate the effects of individual parameters due to the complexity of specimens utilised and limitations of 3D-printing software. Obviously, modification of multiple manufacturing parameters simultaneously results in overlapping trends; for example, changes in travel speed of the printhead, layer size and nozzle temperature have a combined influence on the temperature of the extruded filaments. There is a need to reduce the complexity of such studies by utilising simple specimen geometries comprising the smallest possible feature (individual extruded filaments) and individual modifications to better characterise the impact of each parameter on resulting properties. In addition to experimental studies, recent investigations used simulations to develop predictive capabilities and new fundamental understanding of mechanical properties [29,30].

Several studies have investigated the fundamental fracture mechanics of 3D-printed parts using specimens comprising of a small number of extruded filaments. Coogan and Kazmer [15] developed a specimen geometry that overcame many of the existing limitations of slicing to allow precise analysis at the scale of individual filaments. Li et al. [31] studied thin specimens with a 1.1 mm wall thickness to study fracture properties. Although numerous studies sought to investigate the effect of interface-bond formation on the strength of 3D-printed parts [6,11,15,16,18,19,28], there are no studies to date explicitly analysing the unavoidable impact of filament-scale geometric stress raisers on interface strength.

It is hypothesised that filament-scale geometric features have a critical effect on the tensile strength of extrusion-based 3D-printed parts. The term *filament-scale geometric features* refers to characteristics at the scale of single extruded filaments; these include the naturally occurring curvature of the extruded-filaments (demonstrated in the inset schematics in Fig. 1(a) and (b)) and any manually applied geometric features of similar size. The present study is the first to directly investigate the role of these features on the fracture of 3D-printed polymers; this was made possible by the development of a novel machine code (G-code) capable of producing a single-extruded filament thickness specimen geometry that allows comparison of specimens that are identical except for the presence or absence of manually-applied geometric stress raisers (which emulate the filament-scale geometric features of bonded filaments). Importantly, this allows the effect of geometric features on mechanical properties and performance of 3D-printed parts to be investigated independently from that of the interface between filaments. Additionally, this study is the first to utilise PLA specimens produced with a single extruded-filament thickness to enable a new level of fundamental understanding of 3D-printed PLA. Results are analysed with respect to natural mechanical anisotropy that exists in extrusion 3D-printed specimens. Anisotropy in this study is considered a phenomenon at the global scale of the produced specimen rather than a complex local (filament-scale) anisotropy of the printed material related to the preferential orientation of polymeric chains. This study develops new fundamental understanding of

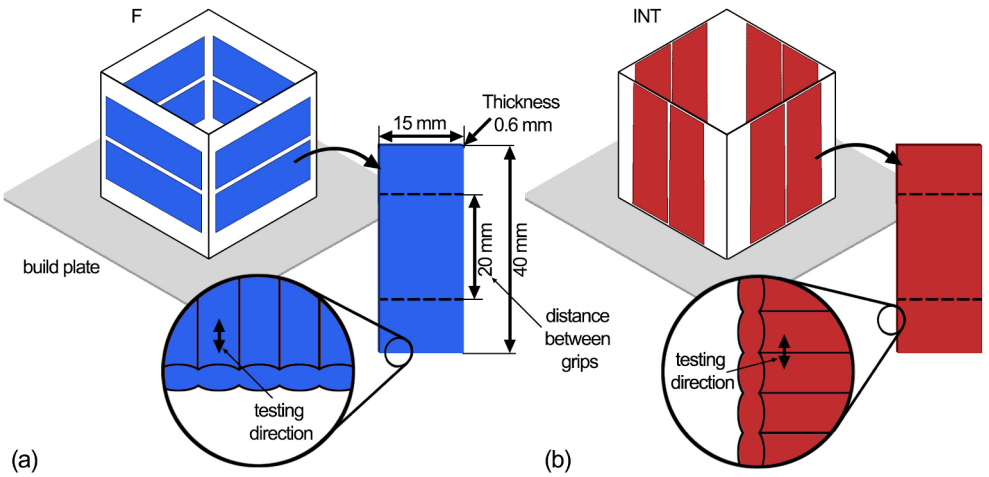

Fig. 1. Schematic of 3D-printed hollow boxes and cut specimens. Eight specimens were cut from each box. Inset sections indicate the orientation of extruded filaments in the filament-direction (F) (a) and interface-direction (INT) (b) specimens. Tensile loads were applied in the filament direction for F specimens and normal to filaments in INT specimens as indicated in the insets of (a) and (b). INT specimens may fail along the interface between 3D-printed layers during fracture testing whereas the fracture crack must pass through each filament for F specimens. Dimensions of all specimens is given in (a) (dashed lines indicate the distance between the grips for tensile testing).

the impact of filament-scale geometric features on interfacial strength, which is widely accepted as critically important but lacks understanding and consensus in the literature. The results are directly applicable to the manufacture of high-precision parts and other high-value manufacturing with extrusion-based 3D-printing.

2. Methods and materials

2.1. The 3D-printing process

Specimens for this study were produced using natural polylactide (PLA) (3DXTECH® branded NatureWorks® polylactide 4043D, Sigma Aldrich) using a RepRap X400 3D-printing system. Single extruded filaments were deposited to form a four-sided hollow box utilised to generate specimens with two different orientations: filament-direction specimens (denoted F) (with filaments oriented in the longitudinal direction) and interface-direction (INT) ones (with filaments oriented in the transverse direction) as shown in Fig. 1 (a) and (b), respectively. The manufactured hollow boxes were generated with wall dimensions of 40 mm (H) × 45 mm (W) and a thickness of 0.6 mm (Fig. 1). A thickness of 0.6 mm was selected as it can be generated with the extrusion of a single extruded filament and is within the range suggested in ASTM D1708 - 18 micro tensile-testing standard method for polymer testing [32]. A 0.4 mm nozzle was utilised with printhead travel speed of 1000 mm min^{-1}. Nozzle temperature was set at 210 °C and the print platform was heated to 60 °C. Custom G-code was developed to manufacture this geometry, providing benefits over typical 3D-printing software by enabling explicit control of:

- printhead speed, ensuring constant speed was maintained across the geometry during extrusion; this was achieved because there were no directional changes at any point within specimens that were ultimately cut from the hollow box as described in Section 2.2.1.
- printhead extrusion rate, ensuring the same volume of material was deposited at all regions across the geometry.
- direction, ensuring no variability in filament orientation and a set transition point between layers.
- cooling time, ensuring the time between material being extruded on one layer and the next was constant for all positions within every layer; this reduced thermal variation and was only possible because all filaments were extruded directly above those on lower layers.

2.2. Specimen preparation

2.2.1. Cutting the specimens

Two types of specimen were cut from the 3D-printed hollow boxes: filament-direction (F) specimens, which were mechanically loaded along the extruded-filament direction, and interface-direction (INT) specimens, which were mechanically loaded normal to the filament direction (i.e. separating layers). Both types of specimen were cut from identical hollow boxes (Fig. 1), with the only difference between F and INT specimens being the orientation of the blade during cutting. This was achieved by respective adjustments to the cutting process, with the following stages: (i) all boxes were cut at the corners using razor blades to yield four identical flat walls; (ii) the four walls were then mounted into a custom-manufactured jig and cut with razor blades to yield two specimens per wall, as demonstrated in Fig. 1. The dimensions of all specimen types were 40 mm (H) × 15 mm (W) × 0.6 mm (T), and the distance between grips for tensile testing was 20 mm (Fig. 1). A 12-tonne press was used to ensure even and controlled cutting pressure across all specimens; a new blade was used for each hollow box. Each box yielded eight specimens, with six specimens used for mechanical characterisation. In total, thirty-two specimens were prepared, twenty-four specimens in the filament direction (sixteen of which had grooves introduced manually as described in Section 2.2.2) and eight specimens prepared in the interface direction.

2.2.2. Specimen notching and manual introduction of grooves

All specimens were additionally cut using a double-edged craft knife blade at the central point of the longest edge, to generate a 3 mm notch as shown in the schematics of the overall specimens to the top left of Fig. 2(a) and (b). It was hypothesised that filament-scale geometric features in INT specimens (grooves between filaments) introduce stress raisers. To test this hypothesis, sixteen F specimens were scored with a double-edged craft knife (with a blade angle of 22.5°) to introduce a groove feature of similar size to that of the grooves naturally present between 3D-printed layers (inset schematics in Fig. 2(a)). To apply the score, the blade was pulled across the specimens with no downward pressure aside from the weight of the knife. To determine the angle of the filament-scale geometric features (manually applied groove and interface bonds), fifteen introduced grooves and fifteen interface bonds were measured using optical microscopy and ImageJ software; mean values were calculated for both groups. The twenty-four F specimens were divided into three subgroups of eight specimens each: non-grooved (F_{NG}), single-grooved (F_{SG}) and double-grooved (F_{DG}). F_{SG} and F_{DG} specimens were scored horizontally with a blade at the central point across the face as demonstrated in Fig. 2(a); the former had manual grooves introduced across a single face, while F_{DG} specimens had grooves introduced across both faces. Aside from the 3 mm notch, no modification was made to F_{NG} or INT specimens.

2.3. Mechanical characterisation

Tensile testing was carried out using an Instron 5944 testing system with a 2 kN load cell. A strain rate of 0.03 min^{-1} was used in

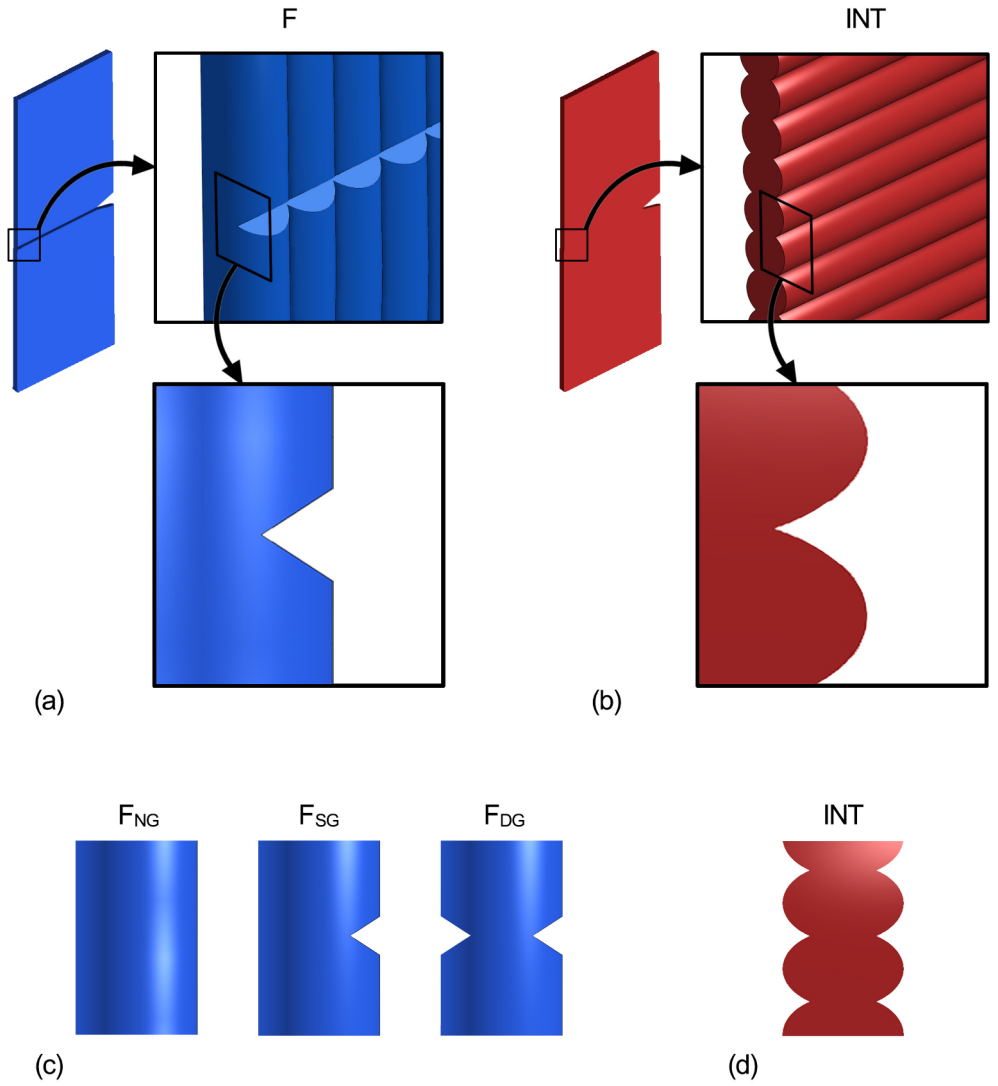

Fig. 2. (a) A filament-scale groove feature was manually applied across all extruded filaments in some F specimens to achieve a filament-scale geometric feature that replicates the naturally occurring groove between 3D-printed filaments in INT specimens (b). (c) The three sets of F specimens were: non-grooved (F_{NG}), single-grooved (F_{SG}) and double-grooved (F_{DG}). (d) INT specimens naturally contained grooves between each extruded filament.

tests; it was chosen to allow observation of the crack propagation. The tensile testing undertaken was displacement controlled, with a displacement rate of 0.5 mm^{-1}; no preload was used. As instantaneous fracture was observed in all but one of the specimen types tested, fracture-resistance curves were not utilised in this study. A Thermosensorik CMT 384 infrared (IR) thermal imaging camera was utilised to record the fracture progression.

2.4. Fracture-surface characterisation

Analysis of fracture surfaces was undertaken using a Zeiss Primotech optical microscope with a 5x magnification lens and an Alicona Infinite Focus measurement system to generate digital coordinates of the fracture surfaces. The plots were post-processed using MountainsMap Premium 7.4 software with amplification set to 20% for all specimens.

3. Results and analysis

This section describes the results of mechanical testing for the four different types of specimens with two main objectives. The first was to determine the effect of filament orientation on mechanical properties. This was achieved by comparing specimens with filaments oriented normal to loading (INT) (i.e. the testing direction was transverse to extruded filaments), with those loaded in the

direction of filaments (F_{NG}) (extruded filaments were parallel to the applied force). The second was to determine the effect of stress raisers, with dimensions similar to those of extruded filaments, on mechanical properties by comparing grooved (F_{SG} and F_{DG}) with non-grooved (F_{NG}) specimens. The obtained force-displacement curves were analysed, and the fracture surfaces were characterised with optical microscopy and 3D surface mapping, to understand mechanical properties and fracture mechanisms.

3.1. Mechanical testing

The results of tensile tests demonstrated that the filament-direction non-scored specimens (F_{NG}) (with filaments oriented in the direction of testing) sustained the greatest force of all specimen-types, with a mean peak force of 333 N (Fig. 3(a)). The INT specimens (with filaments oriented transversally, normal to the direction of testing) fractured with lower mean peak force of 243 N (Fig. 3(d)). This anisotropy was seen in several other studies and is widely accepted to be caused by the bond between 3D-printed layers – regions, which are considered weaker than the bulk polymer material [6–14]. However, with the introduction of a single groove, the mean peak force reduced from 333 N in the F_{NG} specimens to 273 N in F_{SG} specimens (Fig. 3(b)), demonstrating that filament-scale geometric features have a critical effect on strength (both specimens were identical except for the presence of the groove). The introduction of two grooves in the F_{DG} specimen, resulted in an even greater reduction in strength, with a mean peak force of 243 N (Fig. 3(c)). Importantly, the mean peak force of F_{DG} specimens was the same as INT specimens (both 243 N), which are the most geometrically similar types of specimens since manual grooves may be considered equivalent to naturally occurring grooves between filaments of adjacent 3D-printed layers. Typical force-displacement curves for all specimen-types are shown in Fig. 3(e), which clearly demonstrates that manually applied grooves shifted the behaviour of F specimens to be similar to INT specimens. Naturally occurring grooves in the INT specimens may be responsible for the anisotropy typically observed. Values of mean peak force and mean displacement to fracture are shown for all specimen-types in Fig. 4(a) and (b). These results indicate that filament-scale geometric features cause the interfacial weakness observed in many studies, and that the interface strength may be close to that of bulk material, providing weaknesses are not introduced by the printing parameters, for example by utilising low nozzle temperatures or insufficient extrusion rates that result in under-extrusion of filament. This finding may have widespread implications for the interpretation of results for anisotropy in 3D-printed parts, and underlying causes of anisotropy. The authors of this study are unaware of any prior studies that have identified this phenomenon.

The F_{NG} specimens exhibited an extended plastic portion of force-displacement curves prior to fracture (Fig. 3(a)). This was the only specimen type to demonstrate this feature and had a mean displacement to fracture of 0.95 mm (the gauge length was 20 mm in all tests). The values for F_{SG}, F_{DG} and INT specimens were significantly lower (0.51, 0.45, and 0.46 mm, respectively) and no plastic portion of the force-displacement curve was observed. These results support the finding above that filament-scale geometric features (manually-applied grooves for F_{SG}/F_{DG} specimens, and natural grooves between filaments for INT specimens) played a critical role as stress raisers. The double-grooved specimens had almost identical mean displacement to fracture as INT specimens (0.45 mm and 0.46 mm respectively) (Fig. 4(b)), supporting the argument that filament-scale geometric features may be the underlying cause of interfacial weakness (as evident in many experimental studies, but not attributed to geometric stress raisers).

To ensure that the findings of this study were not influenced by minor differences in cross-sectional areas of specimen-types, the area of fracture was measured for all specimens to determine peak stress (as opposed to peak force considered above). Results for peak stress support observations from force-displacement curves, as can be seen in Fig. 4(c): the F_{NG} specimen had higher mean peak stress (55.44 MPa) than the INT specimen (49.47 MPa), which was similar to F_{SG} and F_{DG} specimens (48.92 MPa and 49.87 MPa, respectively). This demonstrates that the introduction of just a single stress raiser (manually-applied groove) caused a reduction in the mean strength of filament-direction specimens to that of the INT specimens. Toughness was also calculated for each type by integrating the force-displacement curves of each specimen; the mean for each group was based on the data for six specimens tested (Fig. 4(d)). The F_{NG} specimens had the greatest mean toughness (230.06 Nmm), significantly higher than that of the F_{SG}, F_{DG}, and INT specimens (74.31 Nmm, 61.28 Nmm and 60.55 Nmm respectively). The toughness data also supports the findings observed for mean force and displacement that interfacial weakness is caused by filament-scale geometric features, which concentrate stresses at the interface, rather than by weak bonding between filaments.

3.2. Infrared studies

Infrared (IR) filming was undertaken for qualitative comparison of thermal changes in specimens during the tensile tests and to give an indication of the respective temperature distributions at various stages. Analysis is shown in Fig. 3(f) to (g). In the F_{NG} specimens, loading initially caused the notch to open in the filament direction (Fig. 3(f) A1 to A2). A local increase in temperature at the notch tip was observed (Fig. 3(f) A3), indicating stress concentration; it gradually progressed along the fracture path (Fig. 3(f) A3 to A4). As the crack in the specimen grew, localised necking occurred with a visible region of increased temperature at the middle point along the fracture path, observed on both the upper and lower segments of the specimen (Fig. 3(f) A4). As the fracture approached completion, the changes in temperature demonstrated that force was distributed along the fracture cross-section (Fig. 3(f) A5). At completion of fracture (Fig. 3(f) A6), higher temperature was localised at the end of the fracture path, evidencing increased stress concentration on the small number of remaining filaments as they underwent fracture. In support of the analysis of force-displacement curves above, introduction of manually applied grooves to the filament direction specimens (F_{SG} and F_{DG}) altered the character of fracture, producing a similar result to that of the INT specimens and significantly different from that observed for the non-grooved specimens. The F_{SG}, F_{DG} and INT specimens exhibited very small notch opening prior to fracture. They fractured rapidly, with similar temperature distributions and fracture paths, indicative of fracture resulting from localised high stress concentration.

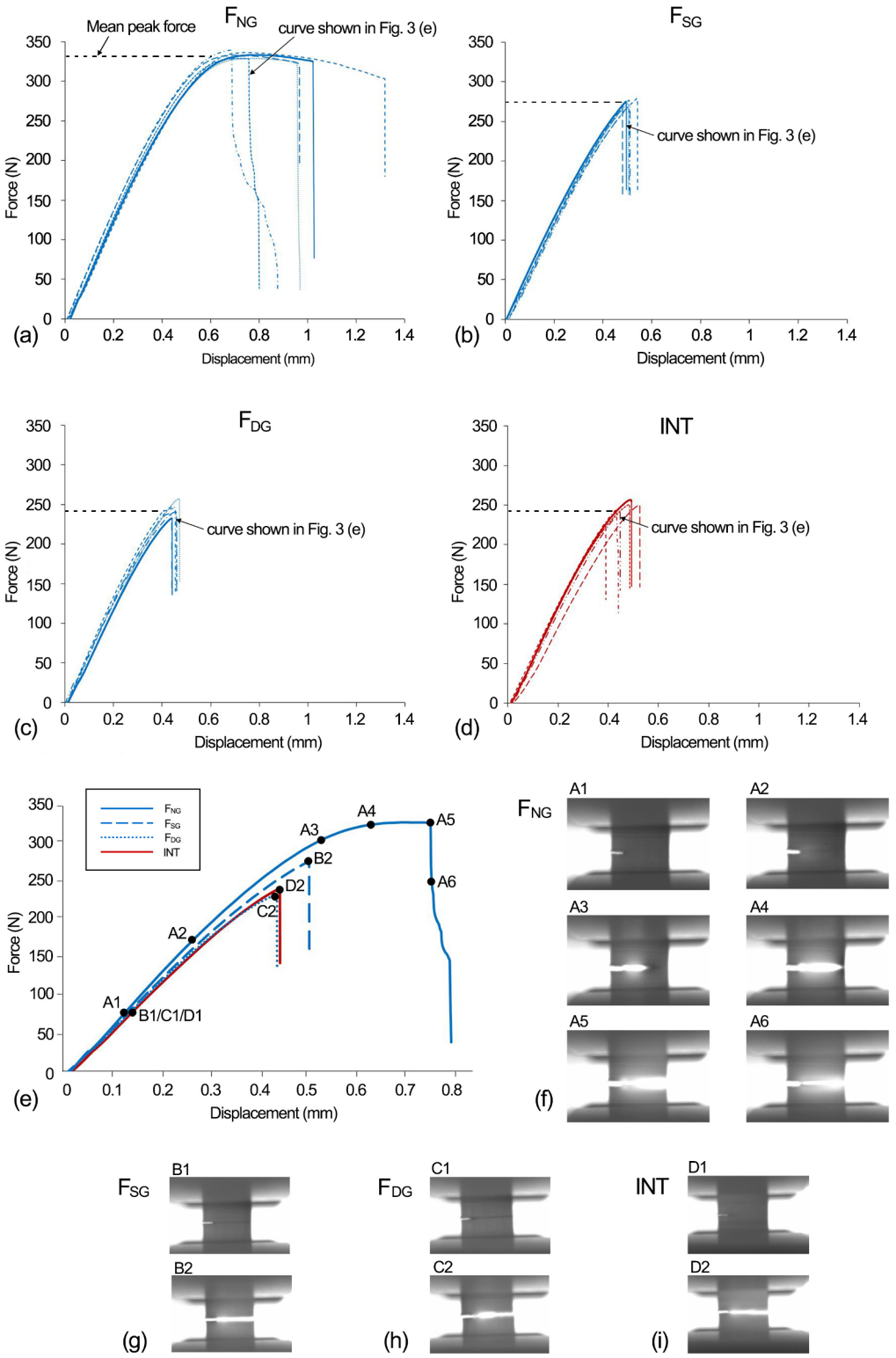

Fig. 3. (a)–(d) Force-displacement curves of F_{NG}, F_{SG}, F_{DG}, and INT specimens indicating the mean peak force. Six specimens were tested for each specimen-type. (e) One example of each of the four specimen-types. (f) – (i) Stages of testing infrared (IR) images for F_{NG} (f), F_{SG} (g), F_{DG} (h) and INT (i) specimens. The region of necking in (f) A4-A6 is shown in close-up in Fig. 8(e).

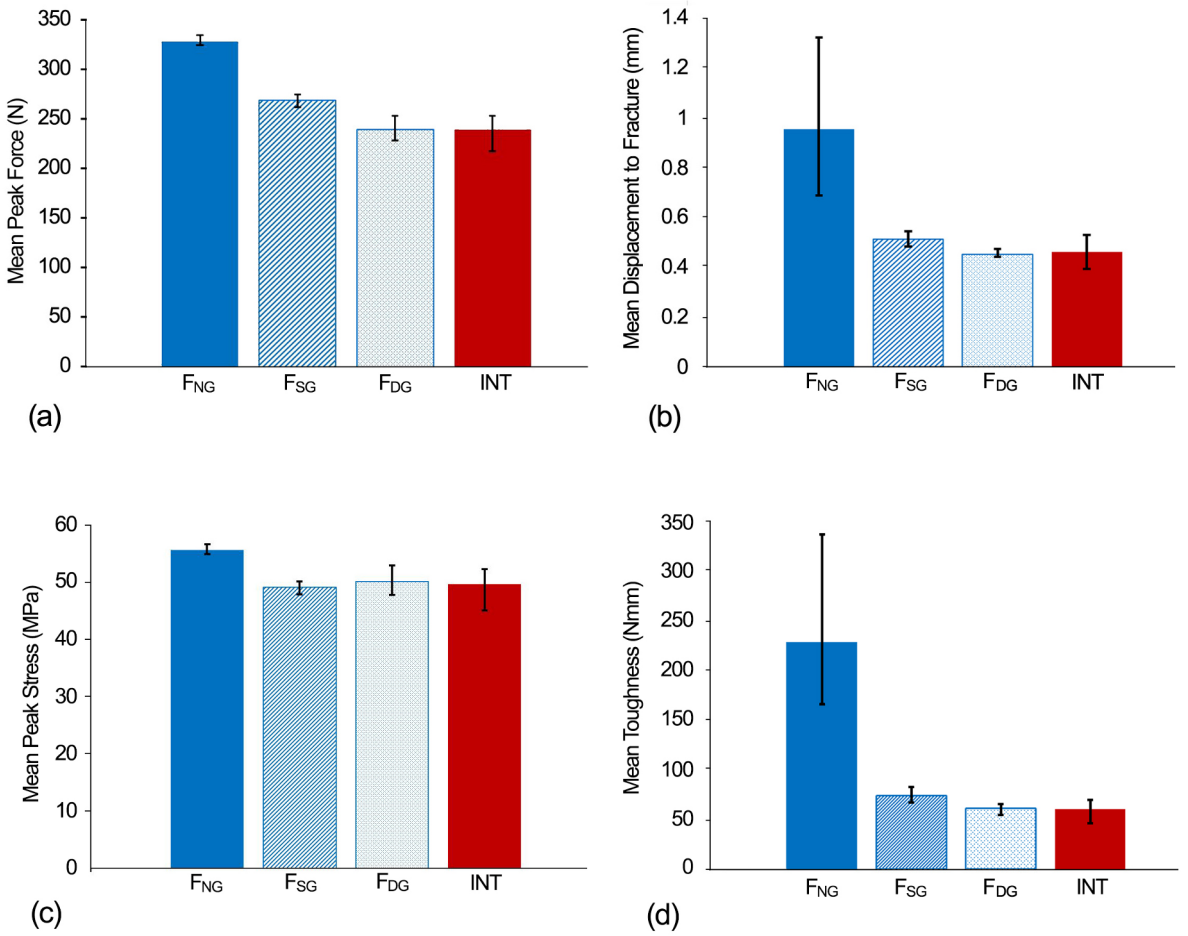

Fig. 4. Mean values of peak force (a) and mean displacement to fracture (b) of 3D-printed specimens. (c) Mean peak stress calculated using areas measured with optical microscopy. (d) Mean toughness of specimens. Error bars indicate the range for six specimens.

This provides further evidence that the grooves (naturally present in INT specimens and manually applied in F_{SG} and F_{DG} specimens) acted as stress raisers, reducing the strength of the specimens.

3.3. Applicability to other 3D-printers

To ensure that the observed trends are characteristic of the extrusion-based 3D-printing process rather than unique to an individual 3D-printer, the F_{NG}, F_{SG}, and F_{DG} specimens were produced from hollow-box specimens manufactured with an alternative 3D-printer (Ultimaker 2 instead of RepRap X400). Four specimens of each type were prepared, stored and tested in an identical manner to RepRap X400 specimens. The same trends were found for specimens made with both printers. The F_{NG} specimens demonstrated the greatest mean peak force (384 N), while the introduction of a single manually-applied groove (F_{SG}) significantly reduced mean peak force (336 N), which was further reduced by the addition of a second groove (F_{DG}) to 317 N. Specimens produced with RepRap X400 demonstrated 86.7% (F_{NG}), 81.3% (F_{SG}) and 76.9% (F_{DG}) of the mean peak force achieved for respective specimens manufactured with Ultimaker 2. The relative reductions in mean peak force by the addition of grooves were 18.0% and 12.5% (single groove) as well as 27.0% and 17.4% (double groove) for the RepRap and Ultimaker systems, respectively. Statistical analysis was undertaken to compare F_{NG} specimens with F_{SG} specimens, and F_{NG} specimens with F_{DG} specimens for each 3D-printing system independently. In all instances the p value was less than 0.005, giving good statistical evidence that findings were consistent and reliable across the two different 3D-printing systems. As with the original 3D-printer, a single groove was sufficient to cause a stress raiser capable of significantly reducing the strength of the specimen. Ultimaker specimens also confirmed another observed trend: the extended plastic portion of force-displacement curves was prevented by the presence of grooves. These findings demonstrate that filament-scale features are an inherent characteristic of extrusion-based 3D-printing, and that all parts manufactured using this method are susceptible to interfacial weakness caused by the stress-raising geometric arrangement of individual filaments.

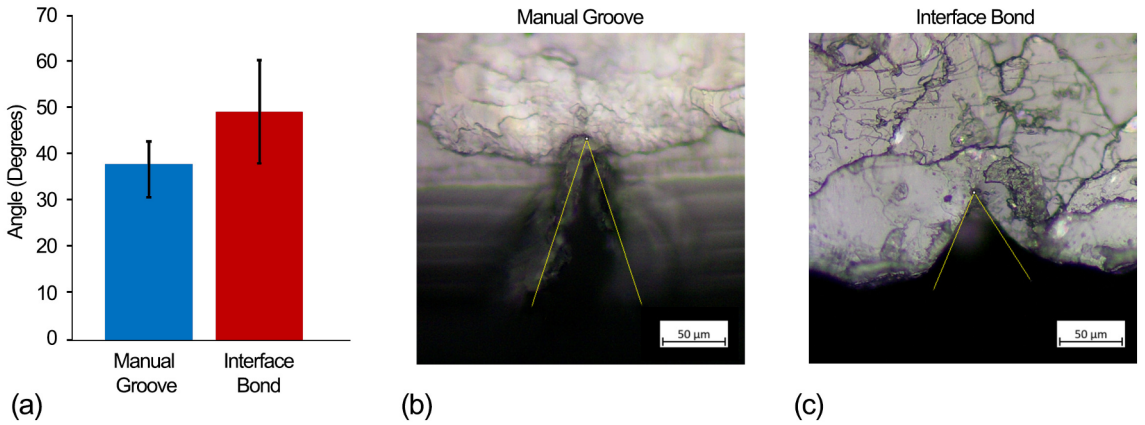

Fig. 5. (a) Mean values for fifteen manual groove angles and fifteen interface bond angles. Error bars indicate the range of measurements. (b) Example of manual groove angle measurement for filament-direction grooved specimens. (c) Example of interface bond angle measurement for interface direction specimens.

3.4. Parameters of manually applied grooves

Optical microscopy and ImageJ software were utilised to measure the angle of the manually applied groove utilised in F_{SG} and F_{DG} specimens as well as the naturally occurring bond angle of the INT specimens (Fig. 5(a) - (c)). In each instance, fifteen measurements were performed, and the mean value was calculated. The manually applied grooves (Fig. 5(b)) were found to have a mean angle of 37.9°; the respective parameter for the naturally occurring bond angles of INT specimens (Fig. 5(c)) was 49.1°. The results demonstrate that on average the manually applied grooves in $F_{SG/DG}$ specimens had a slightly more acute angle than the naturally occurring angle at the interface between filaments in INT specimens, although the ranges of angles measured do overlap for the manual and natural grooves (Fig. 5(a)). It should be noted that the grooves were not expected to be identical and can be considered to be similar, given the ranges measured. The relative similarity of the two groove types supports the validity of the main findings that filament-scale geometric features have an impact of reducing part strength and that it is likely that such features are a major cause of anisotropy in 3D-printed parts.

3.5. Fracture-surface morphology

Analysis of the fracture surfaces (Fig. 6) was used to gain further understanding of failure of the 3D-printed biopolymer. The direction of extruded filaments can be distinguished by the presence of the curved external surface (normal to the fracture surface) at the top and bottom of Fig. 6(a) - (c) distinguishing the F specimens with filaments aligned along the longitudinal axis. In contrast, the INT specimen (Fig. 6(d)) has smooth edges due to the orientation of the extruded filaments along the direction of fracture (transverse to the direction of deposited filaments). Manually-applied grooves were even and consistent, as can be seen in Fig. 6(b) and (c).

Apparently, stress raisers in F_{SG}, F_{DG}, and INT specimens resulted in much coarser texture of fracture surface (Fig. 6(b) - (d)) compared to that of the F_{NG} specimens, with a much smoother surface (Fig. 6(a)). This indicates that although the propagating crack has crossed multiple bond points of filaments along the fracture path, no apparent delamination was initiated. This suggests that the material in the bond regions have comparable fracture toughness to that of the bulk filament and supports the observation that interfacial weakness is a product of the filament-scale geometric features present in the interfacial region, rather than a property of bonding. To enable more detailed analysis of failure, a specimen of each type was scanned along the entire fracture surface using the Alicona Infinite Focus measurement system. The obtained three-dimensional plots of fracture surface were studied in full, and representative middle regions were extracted from each of the plots (Fig. 7). Shear lips were found along both edges of the F_{NG} fracture surface (Fig. 7(a)), with material necking locally to form peaks. This resulted in the characteristic extended plastic deformation seen in force-displacement curves for the F_{NG} specimens (Fig. 3(a)). The consistency and symmetry of the features are more apparent when analysed in the cross-sectional profile (Fig. 8(c)). Shear lips were only observed toward the edges of extruded filaments. However, they were not observed in the F_{SG} fracture surface (Fig. 7(b)), although one edge of this specimen (without the groove) was the same as in the F_{NG} specimens; this indicates that the introduction of the manually-applied groove was sufficient to prevent necking in the F_{SG} specimens (in contrast to F_{NG} ones). The opposing fracture surfaces of F_{NG} specimens (see schematic in Fig. 8(b)) showed that shear lips formed along both edges and on both opposite fracture surfaces. As a result, the F_{NG} specimens exhibited far greater plasticity than all other specimen-types, which had no apparent necking or shear lips (Fig. 7). Surface roughness (Sa) was measured for the regions defined in Fig. 7 and for the entire extracted plot. Values are indicated on the figure but do not indicate any consistent trends. The results of increased plasticity in the F_{NG} specimens are shown in Fig. 8(e). The specimen exhibited a curved discoloured region indicating the presence of localised necking and crazing that was supported by the IR analysis (the same region exhibited increased temperature during fracture (Fig. 3(f) A4)). This confirms that the introduction of grooves in the F_{SG} and F_{DG} specimens prevented formation of characteristics typical of fracture in F_{NG} specimens. Instead, their fracture characteristics were similar to that

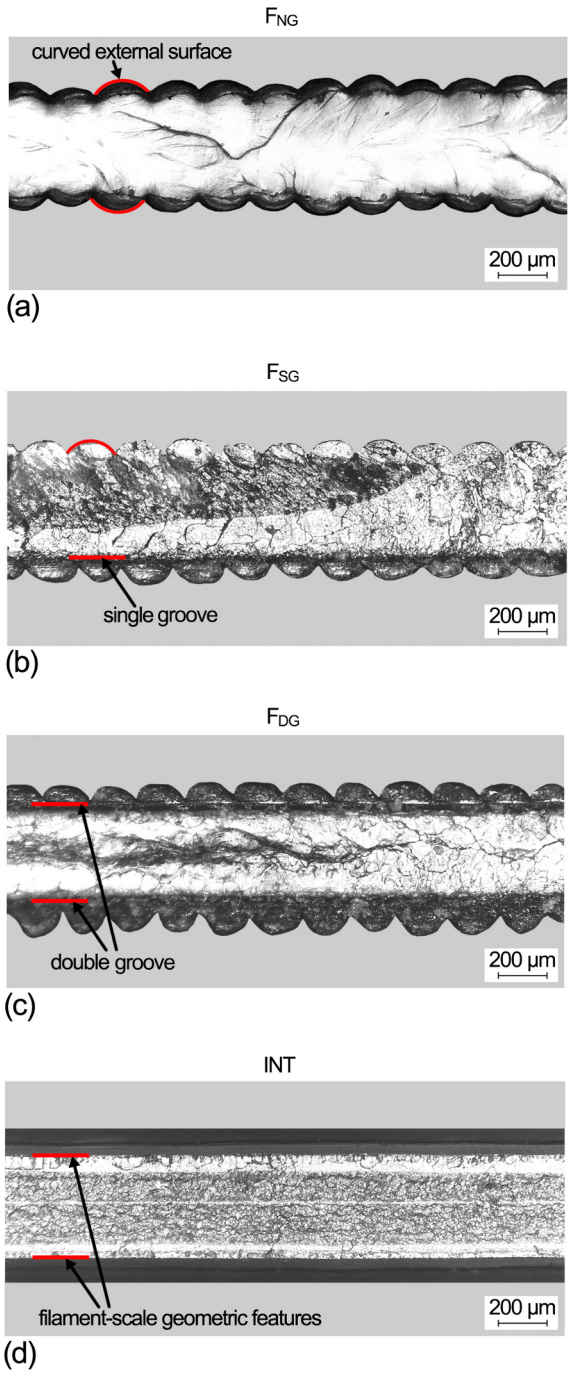

Fig. 6. Optical microscopy of F_{NG} (a), F_{SG} (b), F_{DG} (c), and INT (d) specimens. Filament-scale geometric features include a curved external surface normal to fracture in F specimens (a-b), manually-applied grooves in F_{SG} and F_{DG} (b-c) and naturally-occurring grooves in INT (d).

exhibited by the INT specimens (Fig. 7(b) to (d)). Fractography showed that the filament direction-specimens (F_{NG}) had smoother fracture surface than other specimens (Fig. 6(a)).

Introduction of grooves to the filament direction specimens (F_{SG} and F_{DG}) altered their fracture characteristics, resulting in resemblance to the INT specimens (Fig. 6(b)-(d) and Fig. 7(b)-(d)), indicating that filament-scale groove features have a crucial influence on fracture. The importance of these findings is discussed in the next section.

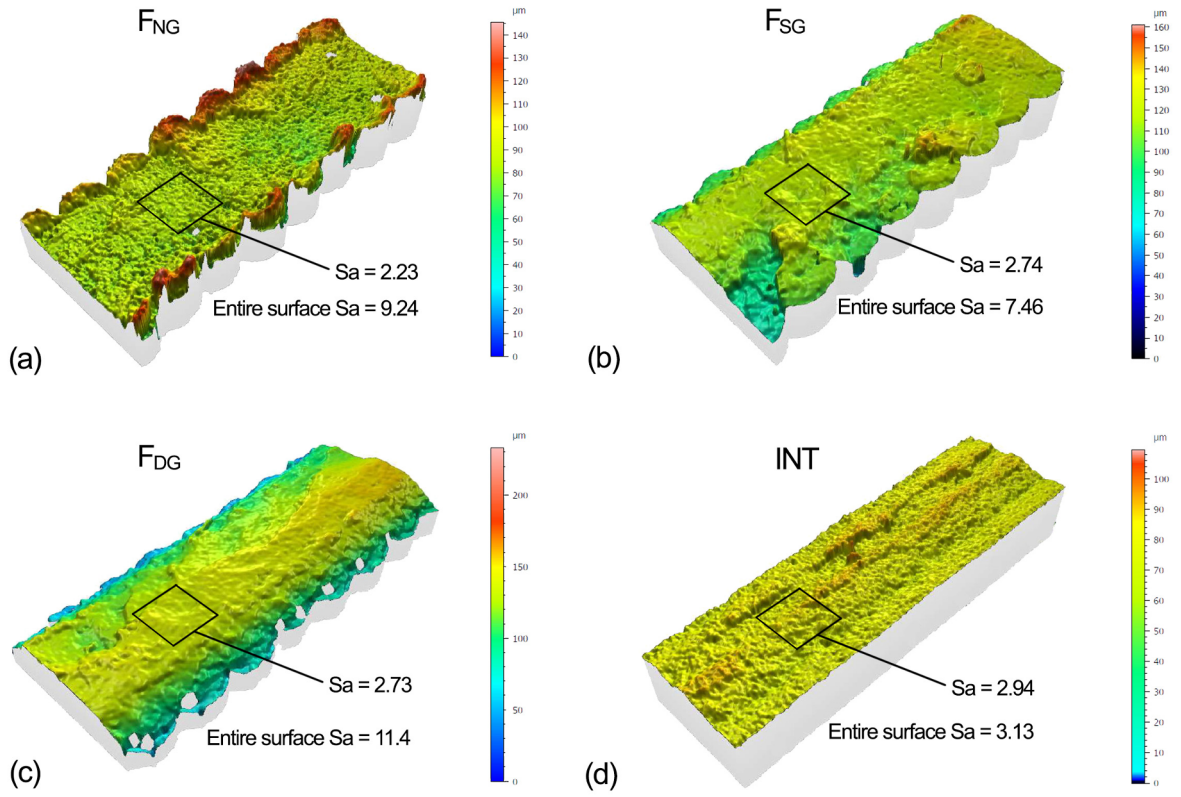

Fig. 7. Extracts of fracture surface plots scanned using the Alicona Infinte Focus system for F_{NG} (a), F_{SG} (b), F_{DG} (c), and INT (d) specimens. Surface roughness (Sa) is given for the inset region and entire surface of each specimen.

4. Discussion

4.1. Filament-scale stress raisers

This study is the first to identify and demonstrate the critical importance of the filament-scale geometric features on mechanical performance of 3D-printed polymeric parts. In addition to identifying the relevance of naturally occurring stress raisers in interface direction, the study showed that introducing manually applied stress raisers had the effect of reducing filament-direction strength in such a way that filament-direction performance becomes very similar to interface direction performance. In other words, the mechanical anisotropy of such parts observed in many studies is a result of these geometrical features, rather than of weak interfaces between filaments. No other studies to date have demonstrated the extent, to which these geometric features influence the mechanical performance. The trends observed in mechanical testing (Section 3.1) demonstrated that the presence of grooves ($F_{SG,}$ F_{DG} and INT specimens) generated stress concentration that reduced strength significantly. A number of studies showed that parts comprised of multiple extruded filaments have internal pores (sometimes described as air gaps) [14,16,22,27,33–35] in regions where multiple filaments are bonded together but have not fundamentally demonstrated the impact of these on mechanical performance by isolating the features as was achieved in this study. Pores formed in the process of bonding of internal filaments resulted in internal filament-scale grooves similar to those considered in this study. As this study demonstrated, an individual groove can drastically weaken parts, it is expected that multi-filament geometries, exhibiting both internal and external grooves, would encounter the same reduced mechanical performance due to stress raisers. Developing software capable of generating toolpath strategies that reduce the incidence of filament-scale grooves would improve the strength of 3D-printed parts. Alternatively, software that optimises filament orientations to minimise the impact of filament-scale stress raisers would also improve part strength.

4.2. Bond strength

The introduction of two manually applied grooves in the F_{DG} specimens was meant to replicate the filament-scale geometric features that naturally occur in INT specimens (demonstrated in Fig. 2(a)-(b)). The force-displacement results (Fig. 4(a)-(b)) and fracture-surface analysis (Fig. 6(c)-(d) and Fig. 7(c)-(d)) demonstrated that these two specimen types had very similar fracture characteristics. This is strong evidence that the material in the fracture regions of both F_{DG} and INT specimens was similar, suggesting that material bond formation at the interface was of comparable quality to the bulk extruded-filament material and therefore not responsible for the observed weaknesses. The manual addition of grooves eliminated anisotropy, which is widely reported for 3D-

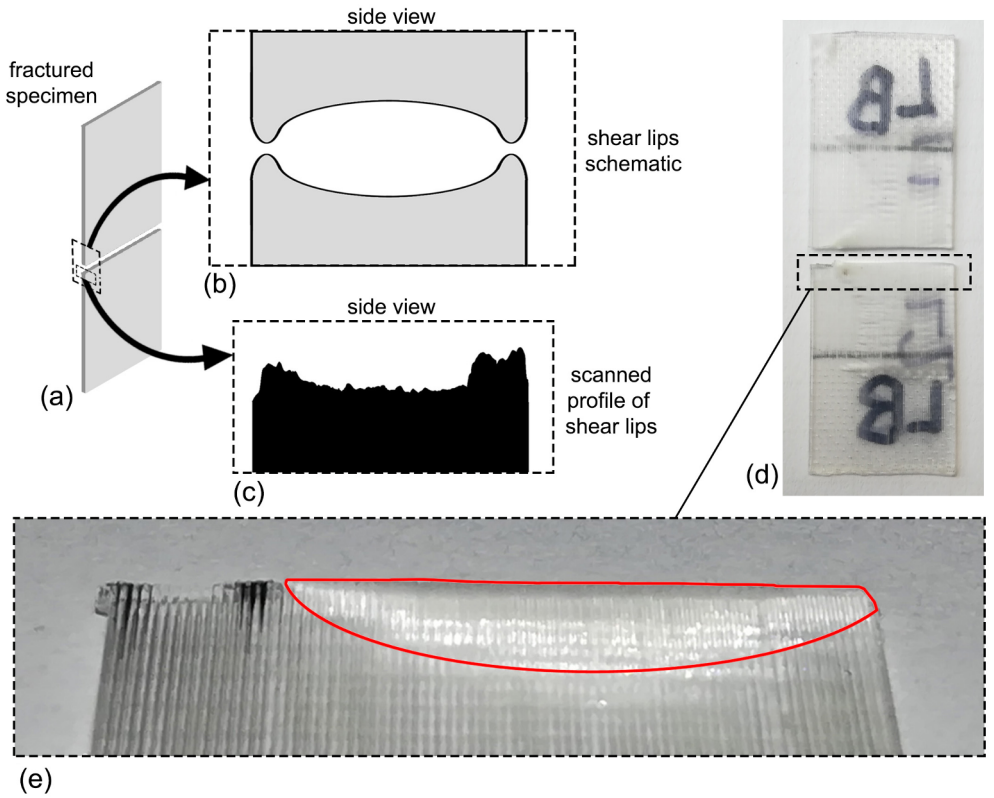

Fig. 8. (a) Schematic of fractured F_{NG} specimens indicating location of side view (b) and side view (c). (b) Schematic of fracture surface profile for F_{NG} specimens demonstrating shear lips necking on both fracture surfaces. (c) Experimentally scanned profile of shear lips based on Alicona data. (d) Fractured specimen with inset figure (e) demonstrating location of observed necking and crazing resulting from fracture of F_{NG} specimens.

printed specimens. It is still important to consider bond strength because bond formation is influenced by many factors (including printing temperature, material and print duration of each layer) and some combinations of such parameters may hinder this process. Understanding the role of filament-scale geometric features in fracture is key for control and optimisation of the printing process. Improvement of bond strength is an active research area, but some of the apparent bond weakness reported in the literature may be incorrectly attributed to issues with insufficient bond strength when in fact this can be a symptom of geometric stress raisers as opposed to poor inter-filament bonding. Several works on theoretical bond formation [36,37] found complete bond healing over very short time periods, supporting the theory that bond strengths are very similar to that achievable in extruded filaments.

4.3. Shear lips

The F_{NG} specimens were the only specimen type to demonstrate shear-lip necking at the fracture surface (Fig. 7(a)). Shear lips formed along free surfaces (Fig. 8(c)) and resulted in improved specimen toughness (Fig. 3(a)). This understanding is important as it provides a possibility to improve toughness by optimisation of the printing strategy. This can be achieved with two methods: (i) loading in the direction of extruded filaments (to avoid filament-scale stress raisers), or (ii) development of a new deposition strategy capable of extruding filaments in an arrangement enhancing these characteristics. The latter, for example, is possible with the use of more complex geometrical toolpath strategies or more sophisticated machine control. This is the topic of our ongoing research and future publications. New understanding and continued studies can help to overcome these challenges by informing new printing strategies.

4.4. Applicability to medical and other high-value manufacturing fields

Extrusion-based 3D-printing provides numerous benefits to medical-device manufacturing; parts can be rapidly generated and modified to meet patient-specific requirements. Interfacial weakness that causes anisotropy is a major hindrance to mechanical performance. This study is the first to show that mechanical properties and performance are dependent on filament-scale geometric features. Thus, the novel findings in this study indicate that further investigation can help to develop new print path strategies that can overcome these issues and enable more advanced and highly intricate medical devices with enhanced mechanical properties. Improvements of toughness and fracture toughness by control of filament-scale features is extremely important for medical implants,

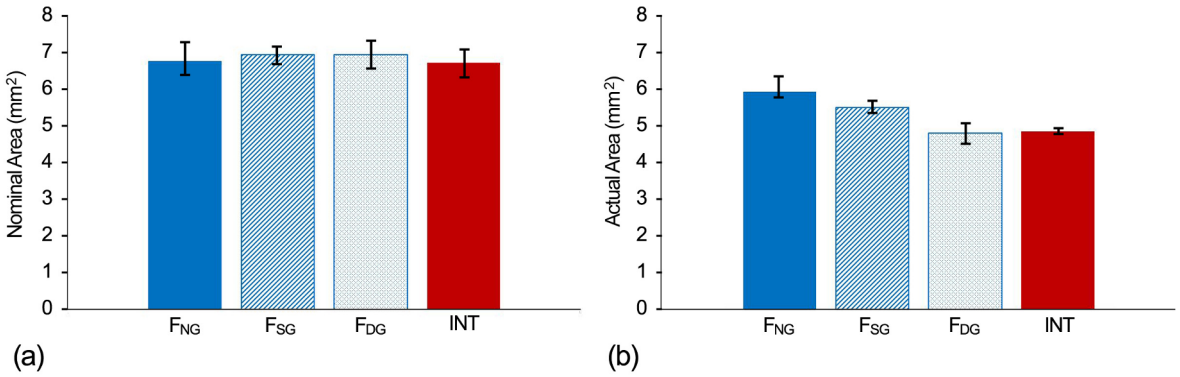

Fig. 9. Mean fracture areas calculated using measurements with digital calipers (a) and microscopy measurements (b) (Error bars indicate the range.).

where failures may have life-threatening consequences and require medical interventions. Similarly, as this study demonstrates, inclusion of just a single groove (or defect) is sufficient to cause a significant reduction in part strength. This suggests that a single incidence of damage to a part manufactured with extrusion-based 3D-printing could have the impact of reducing strength by causing stress concentration.

4.5. Measurement of cross-sectional area – applicability to research and industry

In this study, prior to undertaking the testing program, cross-sectional areas of specimens were assessed using two methods of measurement: digital calipers and optical microscopy. A Zeiss Primotech optical microscope with a 5x magnification lens was utilised in conjunction with ImageJ software for optical microscopy measurement. Caliper-based measurements were found to be misleading as they systematically overestimate the area, depending on orientation of the extruded filaments and the presence of filament-scale geometric features. Importantly, such nominal areas are used in many publications [38,39,40]. Digital calipers are unable to distinguish features such as curvature of extruded filaments, whereas microscopy enables these features to be observed, resulting in the *actual* area to be measured. As demonstrated in Fig. 9, the calculated areas vary depending on the measurement method used. Analysis of the two different approaches to calculating fracture surface area shows that there is a significant difference between calculations based on measurements with digital calipers and optical microscopy for all specimen-types considered here. In the F_{NG} specimens, mean surface area was calculated to be 6.83 mm^2 when utilising digital calipers and 6.01 mm^2 when using microscopy, a difference of 0.82 mm^2 (12%). The difference in the F_{SG} mean surface area for the two methods is greater than that for the F_{NG} specimens, yielding 7.01 mm^2 using digital calipers and 5.59 mm^2 using microscopy. For the F_{DG} specimens mean surface area was calculated at 7.01 mm^2 using digital calipers and a significantly lower 4.88 mm^2 using microscopy, demonstrating a large difference of 30.4%. The same trend was observed for the INT specimens, with a difference of 27.2%. This demonstrates the importance of microscopic measurement, when comparing specimens with different extruded filament orientations or filament-scale geometric features since traditional measurements with digital calipers may provide incorrect results or misleading trends. Optical microscopy was utilised in this study.

5. Conclusions

This study found that grooves occurring naturally between extruded filaments play a critical role as stress raisers and reduce the strength of 3D-printed polymer parts. Specimens that were mechanically loaded in the direction of extruded filaments (F) (longitudinal specimens) were stronger than those loaded normal to this direction (INT) (transverse specimens) (for which delamination of weak filament-bonds is widely accepted as the dominant cause of failure). However, the introduction of manually applied grooves to specimens loaded in the filament direction (to emulate the filament-scale geometric features occurring between bonded filaments) drastically reduced their strength, weakening the specimens to the extent of elimination of anisotropy and making them indistinguishable from specimens loaded normal to the filament direction. Manually-applied grooves also drastically reduced the mechanical toughness of specimens loaded in the filament direction by up to 73%, rendering their displacement characteristics near identical to those of specimens loaded normal to the filament direction. Previous studies attempted to show that inadequate bond formation in extrusion-based 3D-printing results in bond weakness, proposing this as the biggest factor causing the reduction in material properties at the interface region [6,14–26,28,29]. This study provides comprehensive evidence that filament-scale geometric features may play a more important role than inter-filament bonding, providing suitable 3D-printing conditions and parameters are utilised. Findings were corroborated on a second 3D-printer (from a different manufacturer) demonstrating broad applicability to the extrusion 3D-printing field. The results indicate that, for the manufacturing conditions used in this study, bond formation at the interface between filaments is not responsible for interfacial and inter-layer weakness: bonds demonstrated mechanical characteristics similar to the bulk extruded-filament material. However, it is important to note that interfacial weakness may be introduced by suboptimal manufacturing conditions such as low extrusion temperatures. The interface region was predominantly

weakened due to the presence of filament-scale geometric grooves, acting as stress raisers and reducing the force required to cause fracture.

These findings are important for understanding and optimising print-toolpath strategies, since they directly control the resulting filament-scale geometric features in extrusion-based 3D-printing. Thus, there is a need for development of 3D-printing strategies based on the new understanding acquired here in order to minimise detrimental effects of filament-scale geometric stress raisers. Overcoming this weakness can vastly improve the mechanical performance capabilities of parts manufactured by extrusion-based 3D-printing, crucial for modern biomedical applications. Additionally, the new understanding will aid interpretation of results in historic and future studies of anisotropic strength in 3D-printed parts.

References

[1] Honigmann P, Sharma N, Okolo B, Popp U, Msallem B, Thieringer FM. Patient-specific surgical implants made of 3D printed PEEK: Material, technology, and scope of surgical application. Biomed Res Int 2018;2018:1–8.
[2] Wong KC. 3D-printed patient-specific applications in orthopedics. Orthop Res Rev 2016;8:57–66.
[3] Athanasiou K, Agrawal CM, Barber FA, Burkhart SS. Orthopaedic application for PLA–PGA biodegradable polymers. Arthros: J Arthros Related Surg 1998;14:726–37.
[4] Rokkanen PU, et al. Bioabsorbable fixation in orthopaedic surgery and traumatology. Biomaterials 2000;21(24):2607–13.
[5] Gleadall A, Visscher D, Yang J, Thomas D, Segal J. Review of additive manufactured tissue engineering scaffolds: relationship between geometry and performance. Burns Trauma 2018;6:1–16.
[6] Ahn S, Montero M, Odell D, Roundy S, Wright PK. Anisotropic material properties of fused deposition modeling ABS. Rapid Prototyp J 2002;8(4):248–57.
[7] Es-Said OS, Foyos J, Noorani R, Mendelson M, Marloth R, Pregger BA. Effect of layer orientation on mechanical properties of rapid prototyped samples. Mater Manuf Process 2000;15(1):107–22.
[8] Sood AK, Ohdar RK, Mahapatra SS. Improving dimensional accuracy of fused deposition modelling processed part using grey Taguchi method. Mater Design 2009;30:4243–52.
[9] Durgun I, Ertan R. Experimental investigation of FDM process for improvement of mechanical properties and production cost. Rapid Prototyp J 2014;20(3):228–35.
[10] Thomas JP, Rodríguez JF, Renaud JE. Mechanical behavior of acrylonitrile butadiene styrene (ABS) fused deposition materials. Experimental investigation. Rapid Prototyp J Aug. 2001;7(3):148–58.
[11] Riddick JC, Haile MA, Von Wahlde R, Cole DP, Bamiduro O, Johnson TE. Fractographic analysis of tensile failure of acrylonitrile-butadiene-styrene fabricated by fused deposition modeling. Addit Manuf 2016;11:49–59.
[12] Kuznetsov VE, Solonin AN, Urzhumtsev OD, Schilling R, Tavitov AG. Strength of PLA components fabricated with fused deposition technology using a desktop 3D printer as a function of geometrical parameters of the process. Polymers (Basel) 2018;10(3):1–11.
[13] Koch C, Van Hulle L, Rudolph N. Investigation of mechanical anisotropy of the fused filament fabrication process via customized tool path generation. Addit Manuf 2017;16:138–45.
[14] Ziemian S, Okwara M, Ziemian CW. Tensile and fatigue behavior of layered acrylonitrile butadiene styrene. Rapid Prototyp J 2015;21(3):270–8.
[15] Coogan TJ, Kazmer DO. Bond and part strength in fused deposition modeling. Rapid Prototyp J 2017;23(2):414–22.
[16] Spoerk M, Arbeiter F, Cajner H, Sapkota J, Holzer C. Parametric optimization of intra- and inter-layer strengths in parts produced by extrusion-based additive manufacturing of poly(lactic acid). J Appl Polym Sci 2017;134(41):1–15.
[17] Reddy BV, Reddy NV, Ghosh A. Fused deposition modelling using direct extrusion. Virtual Phys Prototyp 2007;2(1):51–60.
[18] Aliheidari N, Christ J, Tripuraneni R, Nadimpalli S, Ameli A. Interlayer adhesion and fracture resistance of polymers printed through melt extrusion additive manufacturing process. Mater Des 2018;156:351–61.
[19] Bellehumeur C, Li L. Modeling of bond formation between polymer filaments in the fused deposition modeling process. J Manuf Process 2004;6(2):170–8.
[20] Onwubolu G, Rayegani F. Characterization and optimization of mechanical properties of ABS parts manufactured by the fused deposition modelling process. Int J Manuf Eng 2014;2014:1–13.
[21] Torres J, Cole M, Owji A, DeMastry Z, Gordon AP. An approach for mechanical property optimization of fused deposition modeling with polylactic acid via design of experiments. Rapid Prototyp J 2016;22(2):387–404.
[22] Chacón JM, Caminero MA, García-Plaza E, Núñez PJ. Additive manufacturing of PLA structures using fused deposition modelling: effect of process parameters on mechanical properties and their optimal selection. Mater Des 2017;124:143–57.
[23] Sood AK, Ohdar RK, Mahapatra SS. Parametric appraisal of mechanical property of fused deposition modelling processed parts. Mater Des 2010;31(1):287–95.
[24] Pan AQ, Huang ZF, Guo RJ, Liu J. Effect of FDM process on adhesive strength of polylactic acid(PLA) filament. Key Eng Mater 2015;667:181–6.
[25] Ning F, Cong W, Hu Y, Wang H. Additive manufacturing of carbon fiber-reinforced plastic composites using fused deposition modeling: Effects of process parameters on tensile properties. J Compos Mater Apr. 2016;51(4):451–62.
[26] Christiyan KGJ, Chandrasekhar U, Venkateswarlu K. A study on the influence of process parameters on the Mechanical Properties of 3D printed ABS composite. IOP Conf Ser Mater Sci Eng 2016;114(1):1–8.
[27] Abbott AC, Tandon GP, Bradford RL, Koerner H, Baur JW. Process-structure-property effects on ABS bond strength in fused filament fabrication. Addit Manuf 2018;19:29–38.
[28] Coogan TJ, Kazmer DO. Healing simulation for bond strength prediction of FDM. Rapid Prototyp J 2017;23(3):551–61.
[29] Gleadall A, Ashcroft I, Segal J. VOLCO: A predictive model for 3D printed microarchitecture. Addit Manuf 2018;21(April):605–18.
[30] Gardan J, Makke A, Recho N. Improving the fracture toughness of 3D printed thermoplastic polymers by fused deposition modeling. Int J Fract 2018;210(1–2):1–15.
[31] Li J, Yang S, Li D, Chalivendra V. Numerical and experimental studies of additively manufactured polymers for enhanced fracture properties. Eng Fract Mech 2018;204.
[32] ASTM (D638-02a). American Society for Testing and Materials. Standard test method for tensile properties of plastics (D 638 - 02a). ASTM 2003;08:46–58.
[33] Torrado Perez AR, Roberson DA, Wicker RB. Fracture surface analysis of 3D-printed tensile specimens of novel ABS-based materials. J Fail Anal Prev 2014;14(3):343–53.
[34] Prajapati H, Ravoori D, Woods RL, Jain A. Measurement of anisotropic thermal conductivity and inter-layer thermal contact resistance in polymer fused deposition modeling (FDM). Addit. Manuf. 2018;21(November 2017):84–90.
[35] Huang B, Singamneni S. Adaptive slicing and speed-and time-dependent consolidation mechanisms in fused deposition modeling. Proc Inst Mech Eng Part B J Eng Manuf 2014;228(1):111–26.
[36] Sun Q, Rizvi GM, Bellehumeur CT, Gu P. Effect of processing conditions on the bonding quality of FDM polymer filaments. Rapid Prototyp J 2008;14(2):72–80.
[37] McIlroy C, Olmsted PD. Disentanglement effects on welding behaviour of polymer melts during the fused-filament-fabrication method for additive manufacturing. Polymer (Guildf) 2017;123:376–91.

[38] Laureto JJ, Pearce JM. Anisotropic mechanical property variance between ASTM D638–14 type i and type iv fused filament fabricated specimens. Polym Test 2018;68(April):294–301.
[39] Dawoud M, Taha I, Ebeid SJ. Mechanical behaviour of ABS: An experimental study using FDM and injection moulding techniques. J Manuf Process 2016;21:39–45.
[40] Jayanth N, Senthil P, Prakash C. Effect of chemical treatment on tensile strength and surface roughness of 3D-printed ABS using the FDM process. Virtual Phys Prototyp 2018;13(3):155–63.

Glossary of acronyms

F: filament direction
F_{DG}: filament double-grooved (specimen type)
F_{NG}: filament non-grooved (specimen type)
F_{SG}: filament single-grooved (specimen type)
H: height
INT: interface direction (specimen type)
IR: infrared
PLA: polylactide
PSIs: patient-specific implants
T: thickness
W: width